Shape-Stabilization of Phase Change Materials with Carbon-Conscious Poly(hydroxy)Urethane Foams

Minjung Lee, Samuel D. Dahlhauser, Chloe Lucci, Bryon S. Donohoe, Robert D. Allen, and Nicholas A. Rorrer**

We dedicate this paper to our friend and colleague, Prof. Chris Ober, on the occasion of his retirement from Cornell University. Chris has always been an inspiration to me (RDA) for combining innovation and fundamental understanding in his pursuit of functional polymers for use in challenging applications (semiconductor lithography). We hope that this paper shows the same combination of application-inspired materials innovation and fundamental science.

Thermal energy regulation is a significant challenge, contributing to over 30% of annual greenhouse gas emission (GHG) emissions. Phase change materials (PCMs) offer a promising solution by storing thermal energy, which can enable the reuse of waste heat for heating and cooling; however, developing materials for shape-stabilized PCMs remains crucial. This work investigates a self-foaming poly(hydroxy)urethane (PHU), derived from a non-isocyanate polyurethane (NIPU), as a porous support for shape-stabilizing paraffinic and salt hydrate PCMs. PHU-encapsulated paraffinic PCMs exhibited excellent thermal stability over repeated cycles. Thermal stability with salt hydrate PCMs, specifically calcium chloride hexahydrate ($CaCl_2{\bullet}6H_2O$), is achieved by the incorporation of 5 wt.% barium carbonate ($BaCO_3$) into the PHU foam. This enabled stable cycling for over 48 cycles with desirable thermal properties, i.e., a melting point ≈30 °C, high enthalpy (ca. 138 J g^{-1} per cycle), and a consistent freezing point ≈20 °C, making it suitable for applications in buildings and electric vehicle battery insulation. Also, incorporating graphite (1.5–10 wt.%) into the foam enhanced the thermal conductivity of shape-stabilized $CaCl_2{\bullet}6H_2O$ during heating and cooling cycles. Overall, the approach detailed here offers a carbon-conscious and chemically tunable material for thermal energy storage.

1. Introduction

In modern society, thermal regulation, including heating and cooling, is a significant contributor to energy consumption and GHG emissions. For instance, buildings account for ≈36% of global energy consumption and 39% of CO_2 emissions annually.[1] Of this total, ≈40% is attributed to thermal regulation (e.g., space heating and cooling).[1] Thermal energy storage (TES) technologies play a crucial role in addressing the high energy demand in thermal regulation and improving energy efficiency, particularly for applications in buildings, batteries in electric vehicles (EVs), electronics, and textiles.[2–9] In principle, TES systems can use sensible heat, latent heat, and/or thermochemical energy to regulate temperature.[3] Latent heat storage is the simplest implementation of TES technologies, as latent thermal energy is stored and released through phase transitions including solid-solid, solid-liquid, solid-gas, and liquid-gas transitions.[8] Solid-liquid phase change materials (PCMs) are particularly interesting due to their higher heat of phase transition compared to solid-solid PCMs, with smaller volume changes (≈10%) compared to solid-gas or liquid-gas transitions.[8]

Due to this, PCMs have found applications in thermal regulation in buildings, EV batteries, and in clothing alongside solar heating and air conditioning.[2–10] Organic and inorganic PCMs have advantages and disadvantages, making each more suitable for specific applications. Organic PCMs, such as paraffins, show great cycling stability and chemical inertness but offer low thermal conductivity (ca. 0.1–0.3 W mK^{-1}), moderate flammability, and are expensive in the case of pure paraffin waxes.[10,11] Inorganic PCMs such as salt hydrates are cheap, offer higher energy density (ca. 150–250 J g^{-1}), and good thermal conductivity (ca. 0.5–1.1 W mK^{-1}), but are often corrosive and suffer

M. Lee, S. D. Dahlhauser, C. Lucci, B. S. Donohoe, R. D. Allen, N. A. Rorrer
Renewable Resources and Enabling Sciences Center
National Renewable Energy Laboratory
Golden, Colorado 80401, USA
E-mail: robert.allen@nrel.gov; nicholas.rorrer@nrel.gov

DOI: 10.1002/adfm.202421039

from poor cycling stability and phase separation during temperature swings.[8,11] In particular, some salt hydrates often suffer from incongruent melting[3,8] and other salt hydrates, such as $CaCl_2 \bullet 6H_2O$, suffer from moisture sensitivity and inconsistent nucleation, causing supercooling.[11,12] These unstable melting and freezing behaviors hinder cyclability and thus, practical application.

To overcome the limitations of pure PCMs, various shape stabilization techniques have been developed, such as the use of seeding, nucleating agents, thickening agents, and encapsulants.[12–15] Seeding is performed to provide stable solid crystals from the same material by applying high pressure locally to increase the melting point of only a few particles, whereas nucleating agents are used to add stable solid crystals from compositionally different materials. For encapsulants, nano- and micro-encapsulated PCMs have been widely investigated. In these methods, the PCM core is completely encapsulated within a polymeric or inorganic shell (with a diameter up to 1 µm for nano-encapsulation and less than 1 mm or 1 cm for micro-encapsulation).[16,17] Although these encapsulation processes often succeed in mitigating PCM drawbacks, they can be limited by technically difficult preparations, high manufacturing costs, and potentially low rates of heat transfer.[18,19] In contrast, macro-encapsulation,[20] defined as a process where the PCM capsule size exceeds 1 mm (or 1 cm), offers an attractive approach for PCM stabilization due to its higher heat transfer rates, high loading capacities facilitated by large pore volumes, and potential for incorporating nucleating agents.[12,21,22] Encapsulant materials come in a wide variety, including metals (aluminum, stainless steel, copper), ceramics (silica, calcium carbonate, zinc oxide, alumina), concrete, expanded graphite, and polymers (polyethylene, acrylic-based resins, polyvinyl chloride, polyvinyl alcohol, polyurethanes).[8,15,20,23] Importantly, we need to consider the carbon footprint of the encapsulant within the PCM composite system. This includes a carbon-conscious design of both the PCMs and encapsulant materials to maximize the benefits of PCMs for thermal regulation in reducing GHG emissions and saving energy.[24–27]

Porous materials, often used as encapsulants for PCMs, can offer a large contact area and enhance cycling stability, durability, and thermal conductivity.[13,28] In particular, polymeric foams provide high tunability by controlling pore structure and incorporating additives such as nucleating or thickening agents for the shape-stabilization of PCMs.[13] One example of sustainable porous materials, PHU foams, also referred to as NIPU foams, was recently reported to be self-foaming via chemo- and regioselective addition of thiols and amines to cyclic carbonates, offering a more sustainable alternative to traditional isocyanate-based polyurethanes.[29,30] These PHU foams can be synthesized by the polyaddition of dithiols and diamines with multi-functional 5-membered cyclic carbonates.[29,30] Notably, these 5-membered cyclic carbonates are commonly produced by a CO_2 sequestration approach (i.e., the reaction between epoxy groups and CO_2 via a carbonation reaction).[31] The NIPU's well-documented environmental benefits stem from avoiding the use of toxic isocyanates, and instead utilizing carbon dioxide and feedstocks derived from biomass.[32–38] Further, the foam material is capable of housing nucleating agents and other additives such as nanoparticles, porous minerals, expanded graphite, dispersed salts, and other filler particles, often imparting desirable changes to the physical properties of the foams, as is frequently observed with nanocomposite materials.[39] Furthermore, the PHU foam has been shown to be re-processable, potentially creating circularizable polymer composites.[40–42] *Therefore, it is our view that the PHU foam offers a compelling platform for shape-stabilizing PCMs in net-carbon reduction and energy efficiency applications. To the best of our knowledge, the use of PHU foam as PCM encapsulating material has not yet been demonstrated, despite its attractive benefits, such as a reduced carbon footprint compared to other encapsulants, lightweight properties, and tunable rigidity.*

Herein, we synthesized self-foaming and bio-derivable thermosetting PHU foams for the shape stabilization of both paraffinic and salt hydrate PCMs. We first employed rheology to investigate the synthetic kinetics of the PHU foams. This analysis revealed that the formulation strongly influences the reaction time (relevant to the gel point) and the rigidity of the foam (determined by the final storage modulus). Scanning electron microscopy (SEM) and optical microscopy (OM) confirmed the macro-porous structures of the synthesized PHU foams, with a mixture of open and closed cells. In addition to OM images, in situ OM videos were obtained to demonstrate the well-distributed PCMs throughout the PHU foams, as well as the shape stabilization of PCMs during a melt-freeze cycle. Additionally, differential scanning calorimetry (DSC) measurements indicated that the foams are hygroscopic due to the hydroxy groups, as evidenced by the difference in their glass transition temperatures before and after drying. Thermogravimetric analysis (TGA) revealed two distinct thermal degradation temperatures for the foam, corresponding to the separate decomposition temperatures of the urethane and thioether linkages. After the foam formation and material characterization tests, we infused the PHUs with either organic or inorganic PCMs and evaluated the thermal cycling performance via DSC and temperature change measurements. Paraffinic PCMs (e.g., hexadecane, heptadecane, and octadecane) encapsulated within the PHU foams exhibited stable thermal cyclability without additives. However, the encapsulated salt hydrate PCM, primarily $CaCl_2 \bullet 6H_2O$, displayed no thermal cycling stability in the absence of additives due to its erratic melting and freezing behavior. By dispersing the nucleating agent $BaCO_3$ throughout the PHU foams, we achieved stable thermal cycling for $CaCl_2 \bullet 6H_2O$ for at least 48 cycles. Finally, we explored the incorporation of graphite within the encapsulating PHU foams to enhance thermal conductivity. This approach was evaluated using a thermal conductivity meter and the temperature change measurement. Adding graphite to the foams provides an extra level of control for the widespread implementation of this technology. Overall, this work demonstrates the versatility of the PHU foam platform for encapsulating various PCMs. Beyond shape stabilization, PHU foams offer tunable chemical and mechanical properties through a customizable formulation and variable process approach.

2. Results

2.1. Foam Formulations

To design PHU foams for shape-stabilizing PCM encapsulation, we investigated foam fabrication using self-blowing and

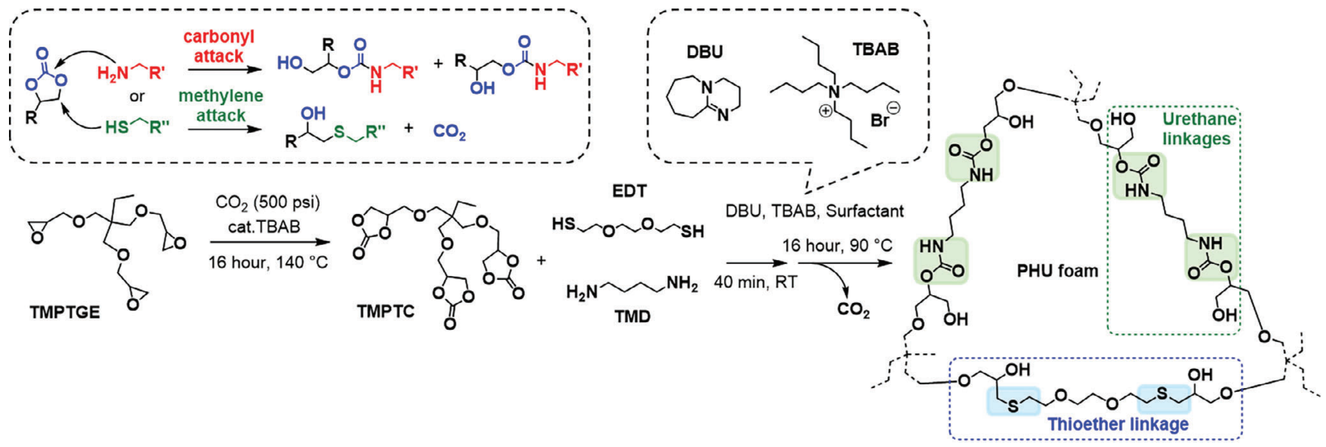

Figure 1. Scheme of PHU foam formation. The synthetic scheme for the formation of the PHU foams used in this work includes the formation of TMPTC precursor by carbonation reaction between TMPTGE and CO_2, and the formation of PHU foam by polyaddition reaction of EDT and TMD to TMPTC. *Abbreviations: PHU, Poly(hydroxy)urethane; TMPTGE, trimethylolpropane triglicydyl ether; TBAB, Tetrabutylammonium bromide; TMPTC, Trimethylpropane tricarbonate; EDT, 2,2-(ethylenedioxy)diethanethiol; TMD, Tetramethylene diamine; DBU, 1,8-diazabicyclo[5.4.0]undec-7-ene.*

carbon-conscious PHU foams. The self-blowing process is enabled by the release of CO_2 via a decarboxylation reaction, preferably when both viscosity and the crosslinking degree of the precured foam mixture are sufficient.[29] Thus, a precure step at room temperature ensures these conditions by allowing partial curing and achieving the desired viscosity level (vide infra). The carbon-conscious nature of the PHU foam stems from several points. First, the PHU foam sequesters more CO_2 throughout its synthesis than it releases in the self-blowing. Also, the PHU foam can exploit bio-based amines[43] such as putrescine, and cadaverine while avoiding the use of phosgene to produce isocyanates, which has significant impacts on GHG emissions, among other environmental health and safety considerations.[44] Specifically, our PHU foams were synthesized via the terpolymerization of difunctional amines (Tetramethylene diamine, TMD) and difunctional thiols (2,2-(ethylenedioxy)diethanethiol, EDT) with a trifunctional cyclic carbonate (Trimethylpropane tricarbonate, TMPTC) in the presence of a base catalyst (1,8-diazabicyclo[5.4.0]undec-7-ene, DBU) (**Figure 1**). This step-growth polymerization involves two distinct reactions: aminolysis and S-alkylation for decarboxylation. Aminolysis occurs through carbonyl attack, while decarboxylation proceeds via thiol-methylene attack. For the monomer selection, TMD, also known as putrescine, was chosen as a bio-derivable diamine that can be produced from a renewable feedstock.[43,45] The use of thiols for an in situ blowing agent can create an unpleasant odor, thus EDT was selected for its low volatility. Our crosslinking monomer, TMPTC, was selected and synthesized due to its ability to sequester a significant amount of CO_2 per gram of starting material (ca. 440 g CO_2 per kilogram of trimethylolpropane triglicydyl ether (TMPTGE)) and the high availability of TMPTGE, the trifunctional starting material (see details on synthesis of TMPTC in the experimental section and ^{1}H-NMR data of TMPTC in Figure S1, Supporting Information). Tetrabutylammonium bromide (TBAB) served both as a carbonation catalyst for the formation of cyclic carbonate from epoxide and as an "foam-aiding reagent" to achieve desirable foam morphologies (vide infra).

Foam formulations were prepared by mixing near-stoichiometric amounts of complementary reactive groups containing TMPTC, EDT, and TMD. The target molar ratio of TMPTC:TMD:EDT was 1:1.025:0.45, resulting in a slight excess (0.05 equivalents) of carbonate functionality relative to the combined amine and thiol functionalities. This excess arises from the ratio of trifunctional carbonate to the sum of difunctional diamine and thiol, which is 3×1:2×(1.025+0.45) or 3:2.95 (≈1:0.983). To this mixture, 0.5 mol% of tetrabutylammonium bromide (TBAB), 10 mol% of DBU, and 0.5 wt.% of silicone surfactant (VORASURF™ DC 5986 from Dow Chemical) were added. Here, TBAB was the residue from the TMPTC synthesis, and the silicone surfactant was used for stabilizing pores during the foaming reaction. An initial screen of thiol versus amine concentrations showed an effective foaming window between 0.4 and 0.45 molar equivalents of EDT, relative to the TMPTC (Figures S2 and S3, Supporting Information). As expected, too little thiol resulted in insufficient decarboxylation and blowing of the thermoset, and too much thiol gave polymers with large, heterogeneously distributed pockets of air (Figure S2, Supporting Information). Although aminolysis and decarboxylation are chemo- and regio-selective reactions, the reaction rate of aminolysis is always higher than the rate of decarboxylation.[29,30] The aminolysis takes place even in catalyst-free or room-temperature environments, whereas the decarboxylation does not occur without a catalyst and is very slow to react in room-temperature environments.[29]

To create a successful foam with uniformly distributed pores, controlling foaming kinetics through the proper viscosity of the reaction mixture was crucial. This was achieved by both formulation and processing. In addition to the tight window of thiol concentration described above, a 40-min precure (i.e., room-temperature aminolysis) following amine addition was implemented. This step induced an easily observable exotherm, partially curing the mixture and ensuring adequate viscosity (see the experimental section for details). This partial curing increased viscosity prior to the final curing at 90 °C, ensuring proper viscosity for uniform bubble growth. As the relative percentage of thiol

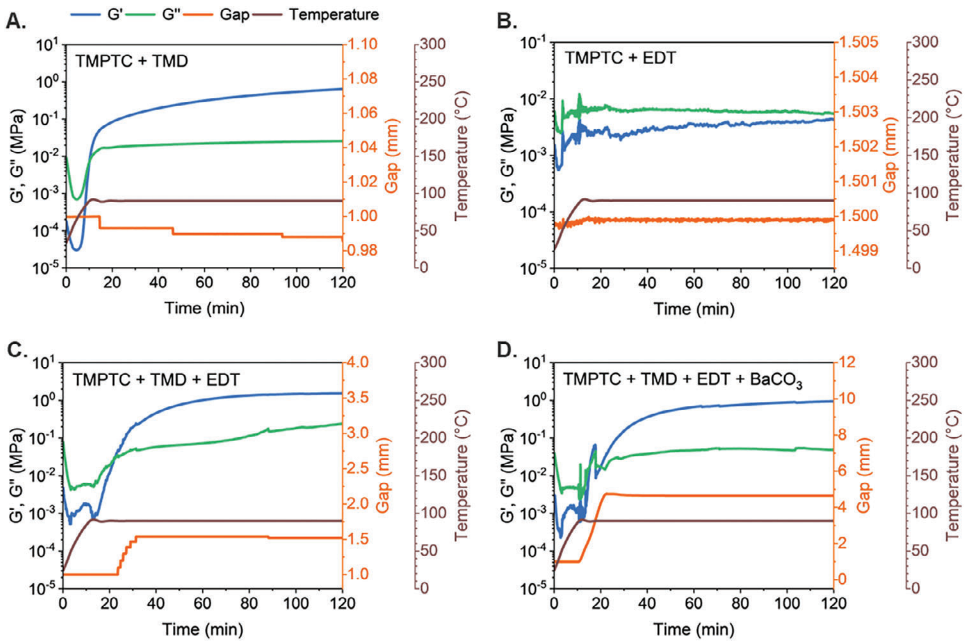

Figure 2. Rheological characterization for monitoring curing behavior of PHU foams. The storage and loss modulus (G′ and G″) evolution of precured mixture with different formulations (A–D) during isothermal curing at 90 °C for the formation of PHU foams. The gap is defined as the height between two parallel plates on the rheometer and measured to observe the foam growth. A) TMPTC and TMD, B) TMPTC and EDT, C) TMPTC, TMD, and EDT, D) TMPTC, TMD, EDT, and 5 wt.% $BaCO_3$ (additive). *TMPTC, Trimethylpropane tricarbonate; TMD, Tetramethylene diamine; EDT, 2,2-(ethylenedioxy)diethanethiol.*

increases and thus the relative percentage of amine decreases, the rate at which the viscosity increases from the precure step is slowed, allowing for cell drainage and coalescence of the air bubbles during the final high-temperature cure. As such, higher thiol concentrations resulted in less dense foams with crumpled foam morphologies (Figure S2, Supporting Information). While screening the foam formulations, the precure, and curing conditions, we observed that residual TBAB content from the synthesis of TMPTC (i.e., the synthesis of cyclic carbonates from CO_2 and epoxides)[46] provided varying foam morphologies even when controlling for stoichiometry, cure time, and cure temperature. Interestingly, the presence of TBAB led to good foam morphology, whereas its absence resulted in a less desirable morphology (Figure S4, Supporting Information). We speculate that TBAB might act as a surfactant or phase transfer catalyst, influencing foam structure. Due to this observed improvement, the formulations retained 0.5 mol% of TBAB remaining from the carbonation reaction as the "foam-aiding reagent".

2.2. Foam Kinetics

To investigate the curing behavior of the PHU foam formulations, we designed a curing experiment at 90 °C in a rheometer. This experiment monitored rheological properties (storage modulus, G′, and loss modulus, G″) during curing and foaming progress by measuring the gap change between parallel plates. Precured mixtures were placed between the rheometer plates (see the setup in Figure S5, Supporting Information). To isolate and study the kinetics of the two reactions (aminolysis and decarboxylation) that contribute to PHU foam formation, different formulations were prepared with the addition of 0.5 mol% TBAB, 10 mol% DBU, and 0.5 wt.% silicone surfactant as shown in **Figure 2**. Additionally, we tested the foaming reaction with a nucleating agent, $BaCO_3$ (5 wt.%), which is expected to aid in the thermal cycling of the salt hydrate PCM used in this study. The detailed reasoning for introducing $BaCO_3$ will be addressed in the section of shape stabilization of PCMs later.

The aminolysis reaction (Figure 2A), the reaction between TMPTC and TMD without EDT exhibited gelation at 10 min indicated by the crossover point of G′ and G″. This was accompanied by a slight decrease in volume over time, observed as a reduction in the gap between the plates. This behavior is attributed to the formation of a cured, non-porous PHU resin due to the absence of a CO_2 release mechanism and thus no foam formation. Surprisingly, the decarboxylation reaction (Figure 2B), the reaction between TMPTC and EDT without TMD, showed no foaming nor gelation even after 120 min at the curing temperature. Furthermore, curing in an oven at the same temperature for 16 h also resulted in no solidification. These observations suggest that TMD plays a critical co-catalytic role in the decarboxylation reaction, in contrast to the previously reported paper[29] about the decarboxylation reaction catalyzed by DBU. While the presence of 10% DBU appears ineffective in catalyzing the thiol-carbonate addition/elimination reaction, its role in accelerating the aminolysis reaction (as previously described)[29] remains important for achieving a successful self-blowing foam.

The foaming reaction (Figure 2C), the reaction of TMPTC, TMD, and EDT using the standard foam formulation, showed a delayed gel point at ca. 22 min compared to the formation of the cured, non-porous PHU resin (Figure 2A), presumably due to the significant offset in stoichiometry to allow for increased thiol

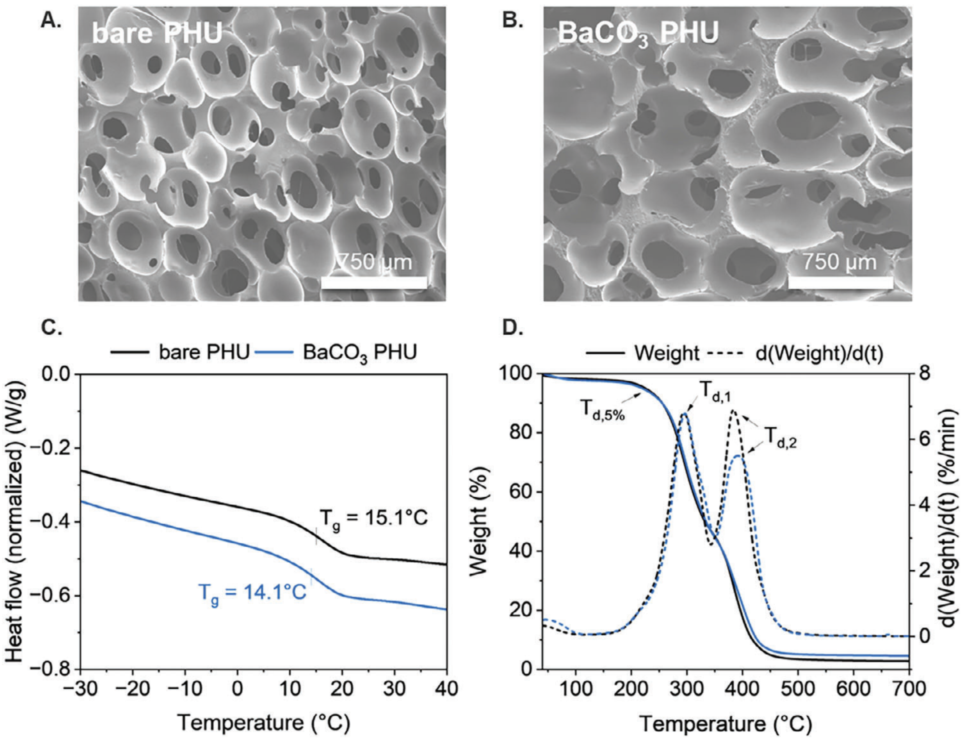

Figure 3. Morphologies and thermal properties of both bare PHU and $BaCO_3$ PHU foams. A) Morphology of bare PHU foam, B) Morphology of $BaCO_3$ PHU foam, both images A and B, obtained via SEM, depict open-cell structures that facilitate PCM infiltration, C) The glass transition temperatures (T_g) of bare PHU and $BaCO_3$ PHU foam, measured by DSC, showing comparable values. D) The thermal degradation temperatures (T_d) of bare PHU and $BaCO_3$ PHU foam, measured by TGA, show comparable thermal degradation behaviors. *$T_{d,\ 5\%}$, thermal degradation temperature at 5 wt.% loss; $T_{d,\ 1}$, the thermal degradation temperature at the first major loss; $T_{d,\ 2}$, the thermal degradation temperature at the second major loss; Bare PHU, PHU without additives; $BaCO_3$ PHU foam, PHU with 5 wt.% $BaCO_3$; SEM, Scanning electron microscopy; DSC, Differential scanning calorimetry; TGA, Thermogravimetric analysis.*

concentration thus lowering the more reactive amine content. Interestingly, the gap change occurred at a similar time, ca. 23 min, and this indicates the foam blowing (CO_2 elimination) begins, just after the gel formation. As G′ almost reached a plateau region ≈120 min, the curing time to obtain a full conversion to a PHU foam could be reduced to 2 h from 16 h. The foaming reaction with a nucleating agent, $BaCO_3$ (Figure 2D), the reaction of TMPTC, TMD, EDT, and 5 wt.% of $BaCO_3$, showed a gel point at ca. 15 min and the onset of the foam blowing at ca. 10 min, which was faster than the foaming reaction without $BaCO_3$ (Figure 2C). The foam with $BaCO_3$ tends to grow faster and larger than the foam without $BaCO_3$, as observed in the trend of gap increase. This enhanced foam expansion in the presence of $BaCO_3$ was also confirmed in foam fabrication without rheometer measurements (Figure S3, Supporting Information), supporting the role of $BaCO_3$ as a nucleating agent for air bubble growth within the foam.

Furthermore, we explored the curing behaviors of PHU foams by varying other parameters such as the curing temperature and the ratio of TMD to EDT (Figures S6 and S7, Supporting Information). As expected, the higher curing temperature led to a faster gel point and foam blowing onset time compared to the lower curing temperature (Figure S6, Supporting Information). Upon varying the ratio of TMD and EDT, the gel point was reached faster by increasing the TMD content, confirming a faster reaction rate of aminolysis compared to decarboxylation as mentioned earlier (Figure S7, Supporting Information). The final modulus, G′, of the foam was higher in the sample with a larger TMD content, suggesting that the urethane linkage is stiffer than the thioether linkage. This is further supported by the higher glass transition temperature measured for PHU foam with a larger TMD content (Figure S8, Supporting Information).

2.3. Foam Characterization: Morphologies and Thermal Properties

The open-cell structure of PHU foams is critical for effective PCM infiltration, as the PCMs need to fill the pores within the foam. The SEM images in **Figure 3A,B** confirmed that our PHU foams contain macropores (both open- and closed-cells) with a relatively uniform pore-size distribution. The average open-cell diameter is 327.04 ± 158.19 µm for bare PHU (PHU without additives) and 298.37 ± 131.64 µm for $BaCO_3$ PHU (PHU with 5 wt.% $BaCO_3$) (see calculation of the average pore diameter in Figure S9, Supporting Information). The cell size is different in $BaCO_3$ PHU relative to bare PHU, as shown in both SEM images (Figure 3A,B) and OM images (Figure S10, Supporting Information), which may affect the shape stabilization of PCMs. Further studies on the effect of cell size and structure will be required.

To evaluate the thermal properties of the foams, the glass transition temperature (T_g) and the thermal degradation temperature

(T_d) were measured by DSC and TGA, respectively. As shown in Figure 3C, the T_g was 15.1 °C for bare PHU and 14.1 °C for $BaCO_3$ PHU, measured after vacuum drying at 60 °C overnight to prevent a hydro-plasticization effect due to the hygroscopic nature of PHU foam. The water absorption under ambient conditions plasticizes the PHU polymer, causing a significant decrease in T_g to 0.9 °C for bare PHU and −2.3 °C for $BaCO_3$ PHU (Figure S11, Supporting Information).[30,47] Furthermore, we confirmed that both bare PHU and $BaCO_3$ PHU can take water up to ca. 40% under a humid environment (Figure S12A,B, Supporting Information). The bare PHU with 40% water uptake exhibited a negative effect (i.e., reduced melting/cooling enthalpies during the thermal cycling of octadecane), whereas the $BaCO_3$ PHU with 40% water uptake showed no significant changes during the thermal cycling of $CaCl_2 \cdot 6H_2O$ compared to the dry $BaCO_3$ PHU (Figure S12C–F and Table S1, Supporting Information). As shown in Figure 3D, the initial decomposition temperatures ($T_{d,5\%}$) were 225.6 °C for bare PHU, and 219.4 °C for $BaCO_3$ PHU. As previously reported for PHUs,[48,49] the two-step thermal degradation took place for our PHU foams via two major mass losses at $T_{d,1}$ = 294.4 °C for bare PHU, 296.1 °C for $BaCO_3$ PHU corresponding to the degradation of the urethane linkages and $T_{d,2}$ = 383.4 °C for bare PHU, 392.3 °C for $BaCO_3$ PHU corresponding to the decomposition of soft segments including the thioether linkages.

2.4. Shape Stabilization of PCMs in Foams

With the PHU foams prepared and characterized, we aimed to investigate their use in the shape stabilization of PCMs. Shape stabilization refers to the process of maintaining the physical structure of PCMs during phase transitions (e.g., melting and freezing). Before understanding the effects of the foams on the shape stabilization of PCMs, we first attempted to study the thermal cycling behaviors of pure PCMs compounds (as received) without the presence of polymeric foams. The organic PCMs studied here, pure paraffin waxes (hexadecane, heptadecane, and octadecane), exhibited stable thermal cycling with comparable enthalpies and narrow melting and freezing peaks (Figure S13A,B, Supporting Information). Conversely, the inorganic PCM, pure $CaCl_2 \bullet 6H_2O$, demonstrated unstable thermal cycles. Depending on its thermal hysteresis, DSC scans showed either no melting or freezing or a single melting peak without subsequent remelting (Figure S13C,D, Supporting Information). As expected, $CaCl_2 \bullet 6H_2O$ particularly requires shape stabilization to demonstrate stable thermal cycles.

We then investigated the performance of PHU-encapsulated PCMs by loading either paraffinic or salt hydrate PCMs into the PHU foams by a simple infiltration method described in the experimental section. The PHU foam was submerged in PCM at a temperature above the melting point of the PCM and then withdrawn to recrystallize the PCM at a temperature below its melting point. While the vacuum infiltration method is commonly used for effective loading of the PCM into the porous materials,[50,51] we found that the simple submersion method without using vacuum works in our PHU foams as evidenced by thermal cycle stability of $CaCl_2 \bullet 6H_2O$ (Figure S14, Supporting Information), probably due to open cell nature of the macropores, with relatively large pore size (ca. 300–330 µm) of the foams (Figure 3A,B) and presumably the chemical affinity between the relatively hydrophilic foam and the PCM in case of $CaCl_2 \bullet 6H_2O$. To illustrate the well-distributed PCMs in both solid and liquid states, we recorded OM videos of PCM melting within various PHU foams from 15 °C to 40 °C (Videos S1–S5, Supporting Information), where the solid PCM appears translucent or hazy, while the liquid PCM appears transparent.

The paraffinic PCMs (hexadecane, heptadecane, and octadecane) were successfully loaded into the bare PHU foams. The weight percentage of paraffinic PCMs in the bare foams was 62.9 ± 2.5% for hexadecane, 64.0 ± 2.1% for heptadecane, and 67.9 ± 0.4% for octadecane. These PHU-encapsulated paraffinic PCMs exhibited stable thermal cycling behavior during 2 DSC heating and cooling cycles (**Figure** 4A). Compared to pure PCMs, the encapsulated PCMs showed somewhat broadened melting and freezing peaks at similar temperatures. We expect to enable a diverse set of potential applications from the wide range of melting/freezing points for these three encapsulated paraffin waxes. Each paraffinic PCM's enthalpies of melting and freezing are presented in Figure 4B. Despite the reduced enthalpies compared to pure PCMs, both melting and freezing enthalpies were comparable to each other, indicating minimal thermal hysteresis or degradation. The calculated energy density (total thermal energy stored) for the paraffinic PCMs in PHU foams was 127.8 ± 0.1 MJ m^{-3} for hexadecane, 106.7 ± 0.9 MJ m^{-3} for heptadecane, and 112.1 ± 0.3 MJ m^{-3} for octadecane based on the measured melting and freezing enthalpies.

Next, one of the salt hydrate PCMs, $CaCl_2 \bullet 6H_2O$, was selected for evaluation of shape-stabilization in this study. This salt hydrate by itself suffers from limitations common to many salt hydrate PCMs, namely incongruent melting, and supercooling, despite its appealing properties such as high energy density (190 J g^{-1}) and ideal melting (ca. 30 °C) and freezing (ca. 20 °C) temperature for applications in buildings and EV batteries.[4,5,52,53] For the PHU-encapsulated $CaCl_2 \bullet 6H_2O$, neither melting and freezing were observed by DSC (Figure 4C), indicating cyclic instability of $CaCl_2 \bullet 6H_2O$ in the bare PHU. The instability of $CaCl_2 \bullet 6H_2O$ typically comes from significant supercooling upon freezing, which can be prevented by introducing additives acting as nucleating agents.[12] Among different nucleating additives, barium salts (e.g., hydroxides, oxides, and carbonates) are known to be effective $CaCl_2 \bullet 6H_2O$ nucleators to suppress supercooling,[22] and $BaCO_3$ was chosen in this study due to facile incorporation to the PHU foam formulation prior to curing process as shown above. In fact, the origin of nucleation was reported in a recent study,[54] which found that a chemical reaction between $BaCO_3$ and $CaCl_2 \bullet 6H_2O$ occurs, generating a solid precipitate that dramatically reduces the supercooling of $CaCl_2 \bullet 6H_2O$. We speculate that the apparent difference in the shape of melting and crystallization peaks stems from this reactivity during recrystallization. With dispersed $BaCO_3$ (5 wt.%) in our PHU foam, $CaCl_2 \bullet 6H_2O$ showed two distinct enthalpies for melting and freezing in DSC (Figure 4D). The calculated energy density of $CaCl_2 \bullet 6H_2O$ in $BaCO_3$ PHU foam was 231.5 ± 4.5 MJ m^{-3} based on the measured melting and freezing enthalpies. The weight percentage of $CaCl_2 \bullet 6H_2O$ in $BaCO_3$ PHU foam was 86.0 ± 0.6%, which is higher than that of the paraffinic PCMs in bare PHU foams. This is due to the higher density of $CaCl_2 \bullet 6H_2O$ (1.7

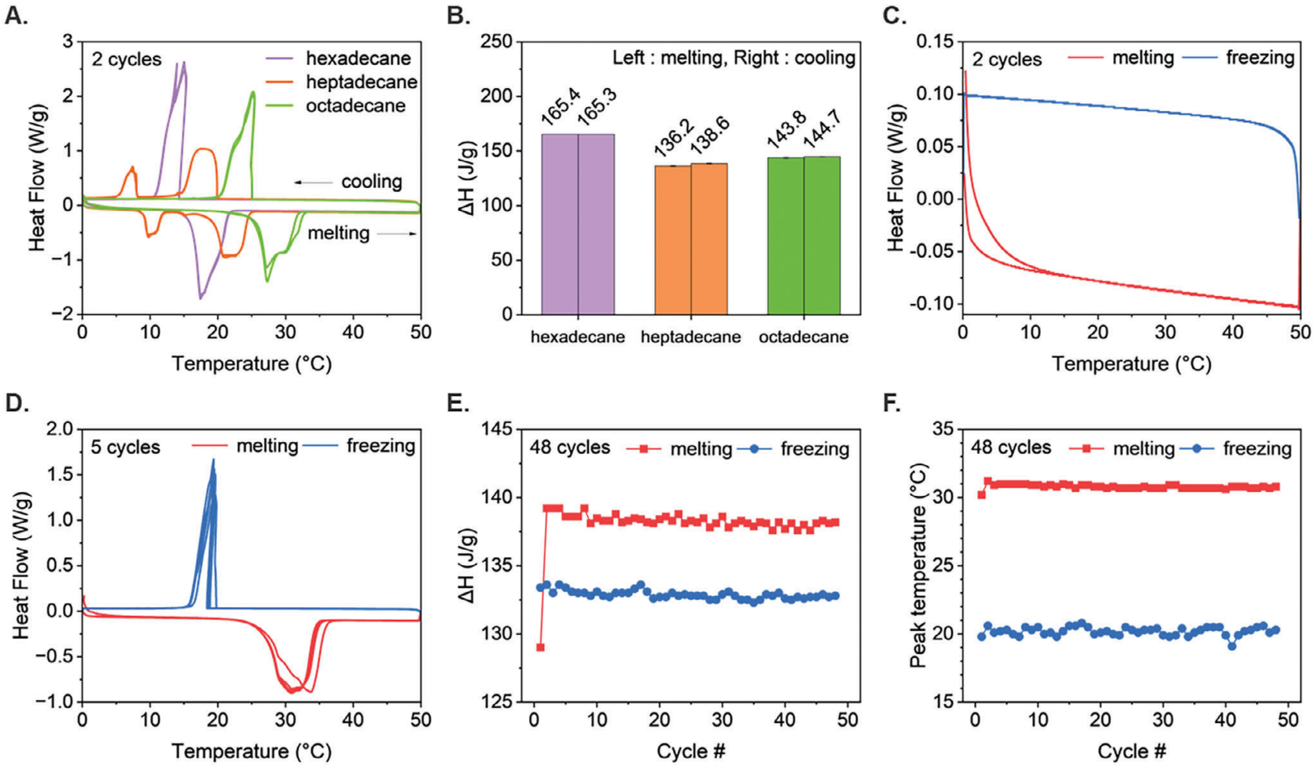

Figure 4. Thermal cycling of PHU-encapsulated PCMs measured by DSC. A) thermal cycling of PHU-encapsulated paraffins including hexadecane, heptadecane, and octadecane during 2 cycles, B) the melting and cooling enthalpies of PHU-encapsulated paraffins extracted from graph A, C) thermal cycling of PHU-encapsulated $CaCl_2{\bullet}6H_2O$ during 2 cycles, D) thermal cycling of $BaCO_3$ PHU-encapsulated $CaCl_2{\bullet}6H_2O$ during 5 cycles, E) the melting and cooling enthalpies of $BaCO_3$ PHU-encapsulated $CaCl_2{\bullet}6H_2O$ during 48 cycles, F) the peak temperatures of $BaCO_3$ PHU-encapsulated $CaCl_2{\bullet}6H_2O$ for melting and cooling during 48 cycles.

g ml^{-1} at 25 °C) compared to the paraffinic PCMs used (0.77–0.78 g ml^{-1} at 25 °C).

Moreover, this $BaCO_3$ PHU-encapsulated $CaCl_2{\bullet}6H_2O$ achieved stable thermal cycling over 48 cycles (the limit of our experiment), though the first melting showed slightly different behaviors compared to the rest of the cycling. Specifically, the enthalpies of melting and freezing remained almost the same (the melting enthalpy = 138.0 ± 0.3 J g^{-1}, the cooling enthalpy = 132.7 ± 0.2 J g^{-1}) during the 48 cycles (Figure 4E). The peak temperatures from melting and freezing also stayed relatively constant (30.7 ± 0.1 °C for melting, and 20.1 ± 0.4 °C for freezing) (Figure 4F). To visualize the shape stabilization of PCMs, we captured in situ videos of $BaCO_3$ PHU-encapsulated $CaCl_2{\bullet}6H_2O$ during melting and freezing using an OM and a digital camera, respectively (Videos S6 and S7, Supporting Information). Additionally, we obtained OM snapshots of $BaCO_3$ PHU before and after the infiltration of $CaCl_2{\bullet}6H_2O$, as well as during a melt-freeze cycle of $CaCl_2{\bullet}6H_2O$ (Figure S15, Supporting Information).

To further evaluate the performance of PHU-encapsulated PCMs, we conducted a temperature change experiment using two reservoirs including a heating bath (hot plate with heating block) and a cooling bath (dry ice/ethylene glycol mixture). Each sample (pure PCMs and PHU-encapsulated PCMs) was placed in a 20 mL glass vial (as detailed in the experimental section) and subjected to 3 consecutive heating and cooling cycles. Each cycle involved 20-min heating at 60 °C and 20-min cooling at ≈-10 °C. A thermocouple placed at the sample center monitored temperature changes during these cycles (Figure S16, Supporting Information). The resulting heating and cooling rates demonstrated effective thermal energy storage and release capabilities of the PCMs at their respective melting (T_m) and crystallization temperatures (T_c), when the PCMs were shape stabilized in PHU foams (**Figure 5**). The thermal energy storage and release of the PCMs were confirmed by the observed heating and cooling delays compared to the PCM-free foam.

The temperature change of pure PCMs without the encapsulating PHU foams was first measured to confirm the melting and freezing behaviors of pure octadecane and pure $CaCl_2{\bullet}6H_2O$ (Figure 5A). Interestingly, the cooling cycles of pure $CaCl_2{\bullet}6H_2O$ showed further lowering of temperature before the onset of the freezing process, which is the supercooling phenomenon described previously.[52] The PHU-encapsulated octadecane exhibited both heating and cooling delays relative to the bare-PHU upon melting and freezing of octadecane for the 3 cycles, indicating stable thermal cyclability of PHU-encapsulated octadecane (Figure 5B). As expected from the absence of both melting and freezing in Figure 4C, the PHU-encapsulated $CaCl_2{\bullet}6H_2O$ (Figure 5C) did not exhibit significant heating and cooling delays since $CaCl_2{\bullet}6H_2O$ is not shape-stabilized. The $BaCO_3$ PHU-encapsulated $CaCl_2{\bullet}6H_2O$ (Figure 5D) exhibited effective heating and cooling delays, consistent with its cyclic

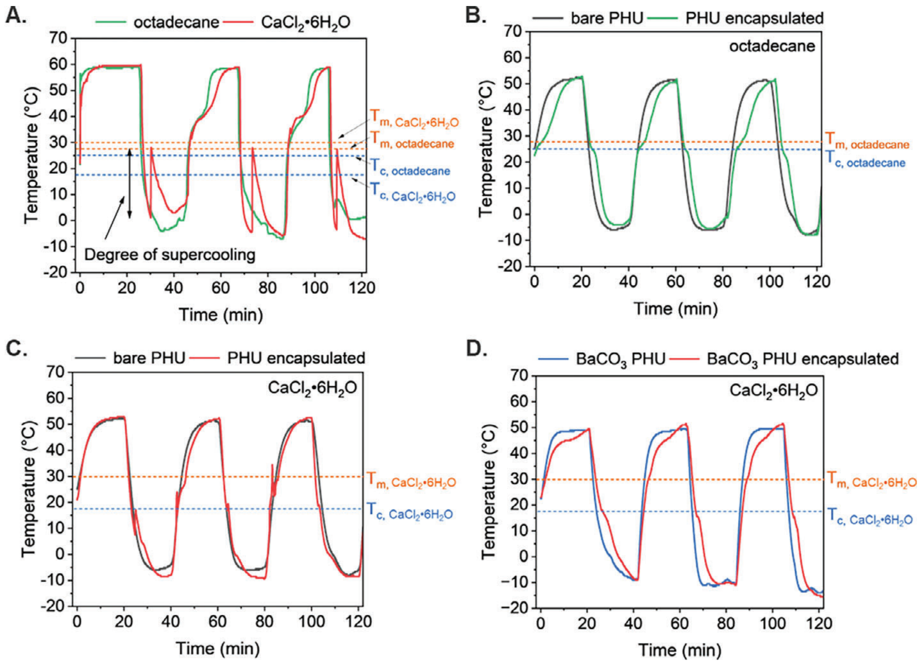

Figure 5. Temperature change of pure PCMs and PHU-encapsulated PCMs upon 3 cycles of heating and cooling. Performance of A) pure PCMs, B) bare PHU and PHU-encapsulated octadecane, C) bare PHU and PHU-encapsulated $CaCl_2 \bullet 6H_2O$, D) $BaCO_3$ PHU and $BaCO_3$ PHU-encapsulated $CaCl_2 \bullet 6H_2O$. Note that the heating of each sample was performed at 60 °C for 20 min on the hot plate and followed by the cooling at ≈−10 °C for 20 min in the cooling bath comprising dry ice and ethylene glycol. *Bare PHU or PHU, PHU foam without additives; $BaCO_3$ PHU, PHU foam with 5 wt.% $BaCO_3$.*

stability observed in Figure 4D. Furthermore, supercooling of $CaCl_2 \bullet 6H_2O$ (Figure 5A) was suppressed in the $BaCO_3$ PHU-encapsulated $CaCl_2 \bullet 6H_2O$, as also evident from the DSC data presented earlier (Figure 4D).

2.5. Thermal Conductivity Enhancement by Incorporating Graphite into Foams

To enhance the thermal conductivity of PHU foams, graphite, a highly thermally conductive material, was readily incorporated during foam fabrication. The thermal conductivity of the 3 different PHU foam formulations (without additives, with 5 wt.% $BaCO_3$, and with 1.5 wt.% graphite and no $BaCO_3$) was measured using a thermal conductivity meter in the temperature range of 0–100 °C (**Figure 6A**). Results showed that incorporating 1.5 wt.% graphite (without $BaCO_3$) did not significantly improve the thermal conductivity compared to bare PHU, except at 100 °C. However, the incorporation of 1.5 wt.% graphite increased the thermal conductivity by an average of 10% across the temperature range relative to $BaCO_3$ PHU. It is important to note that adding $BaCO_3$ to PHU reduces the thermal

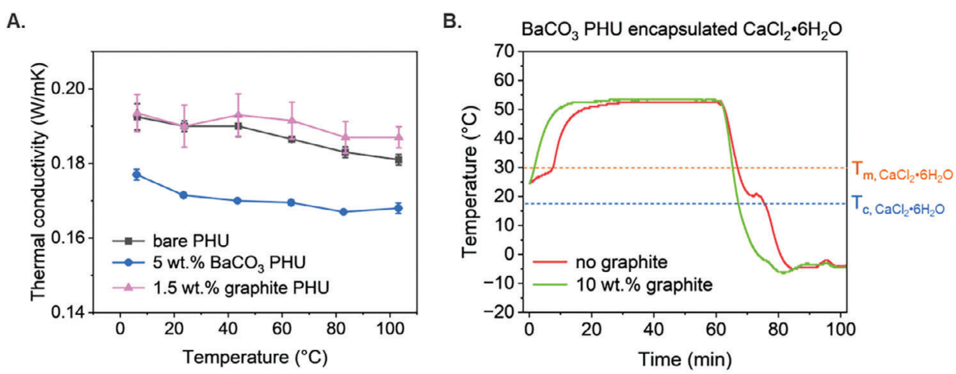

Figure 6. Graphite loading effect on PHU foam. A) thermal conductivity of PHU foams measured by DTC, B) temperature changes of $BaCO_3$ PHU encapsulated $CaCl_2 \bullet 6H_2O$ with or without 10 wt.% graphite upon a cycle of heating and cooling. Note that the heating of each sample was performed at 60 °C for 60 min on the hot plate and followed by the cooling at ≈−10 °C for 40 min in the cooling bath comprising dry ice and ethylene glycol. *Bare PHU, PHU foam without additives; 5 wt.% $BaCO_3$ PHU, PHU foam with 5 wt.% $BaCO_3$.; 1.5 wt.% graphite PHU, PHU foam with 1.5 wt.% graphite and no $BaCO_3$.*

conductivity; however, even a small amount of graphite can compensate for this reduction. Increasing the graphite loading is expected to further enhance thermal conductivity, but measuring samples with higher graphite content is beyond the current scope of this study. Other characterizations of graphite PHU foams with different loadings (1, 5, and 10 wt.%), including morphologies, T_g, density and the thermal cycle of graphite PHU-encapsulated PCM, were performed and are presented in Figures S17–S19 and Table S2-S3 (Supporting Information). Higher graphite loading resulted in smaller cell sizes, as shown in Figure S17 (Supporting Information). Although T_g and thermal cycle behaviors were slightly altered, the shape stabilization of PCM was maintained.

Alternatively, we investigated the impact of higher graphite loading (10 wt.%) on the thermal performance of $BaCO_3$ PHU-encapsulated $CaCl_2{\bullet}6H_2O$ using the previously described temperature change measurement (Figure 6B). The sample with 10 wt.% graphite exhibited an increased heating and cooling rate during a heating and cooling cycle compared to the sample without graphite. In the absence of $BaCO_3$, adding graphite to PHU still increased thermal conductivity, but did not suppress the supercooling of $CaCl_2{\bullet}6H_2O$ (Figure S20, Supporting Information), suggesting that $BaCO_3$ plays an additional synergistic role in mitigating supercooling alongside the enhanced thermal conductivity provided by graphite.

3. Discussion

This work explores the implementation of a versatile PHU foam design as a porous support for shape-stabilizing various PCMs for TES applications. Previous research on polyurethane encapsulants has primarily focused on organic PCMs like paraffins, fatty acids, and alcohols.[15,55–57] Conversely, other polymers such as poly(methyl methacrylate),[58] polyvinyl alcohol,[53,58,59] polyvinyl chloride,[20] and polysaccharides,[60] as well as other materials[13,52,58,61] like porous carbon, mineral, or metal-based materials, have been mainly employed to encapsulate and shape-stabilize inorganic PCMs, including salt hydrates, with a few exceptions using polyurethane foams.[62,63] Interestingly, a recent study on life-cycle GHG emissions for typical building insulation materials revealed that fiberglass produces more than 5 times higher GHG emissions than sprayed polyurethane foam due to higher energy consumption for heating and cooling.[64] Both materials are commonly used for building insulation, particularly in residential in-wall applications in the U.S.[64] While polyurethanes are established encapsulants for PCM shape-stabilization,[55–57,62,65,66] this study is, to our knowledge, possibly the first to utilize PHUs for encapsulation of both organic and inorganic PCMs.

PHUs represent an environmentally friendly class of polyurethanes (non-isocyanate polyurethanes, NIPUs) synthesizable from bio-based resources like lignin and plant oils, replacing petroleum-based chemicals.[67,68] In contrast, traditional polyurethanes are produced from phosgene-based isocyanate precursors such as toluene diisocyanate (TDI) and methylene diisocyanate (MDI), which are energy-intensive to manufacture and have a significant impact on GHG emissions.[44] Notably, PHU synthesis can be "carbon-conscious" due to the cyclic carbonate monomer, derived from CO_2 sequestration via the carbonation reaction between CO_2 and epoxy groups. For PHU foam formation, this study employs a self-blowing process that generates CO_2 (blowing agent) through the decarboxylation reaction between cyclic carbonates and thiols. Importantly, CO_2 consumption outweighs CO_2 generation as only a portion of the cyclic carbonates participate in the decarboxylation reaction with thiols (e.g., CO_2 consumption is almost 3 times higher than generation in molar ratio when the molar ratio of TMPTC:TMD:EDT is 1:1.025:0.45). Additionally, it was reported previously that PHU foams boast sustainable end-of-life options, being melt-reprocessable into PHU bulk films over multiple cycles with fully recovered crosslink density through hydroxyurethane chemistry.[42]

The key to designing PHU foams for specific applications lies in the ease and flexibility of formulation, which dictates final properties like foam rigidity, chemical affinity, and morphology. Successful and controllable foam formation hinges on polymerization and foaming kinetics which are highly sensitive to formulation and process conditions. Control can be achieved through curing conditions (precure time, curing time, and curing temperature) and chemical formulation (stoichiometry of reagents including catalyst, surfactant, and additives, alongside the relative ratio of the main precursors such as cyclic carbonate, thiol, and amine). A primary goal for achieving successful self-blowing PHU foams is ensuring sufficiently high viscosity in precure mixtures before the decarboxylation reaction commences. The aminolysis reaction, influenced by both formulation and curing conditions, is responsible for most of the early viscosity increase. Surfactants play a crucial role in foam stabilization (preventing pore collapse) during the decarboxylation reaction. Additional formulation additives, such as inorganic salts (e.g., $BaCO_3$) and expanded graphite, can tremendously enhance the thermal performance of encapsulated PCMs. The chemical tunability and versatility in incorporating various additives make PHU foams highly beneficial for accommodating diverse PCMs. Furthermore, alternative foaming reactions exist for PHU foam fabrication such as water-induced self-blowing reaction without using thiols,[69,70] catalyst-free and room-temperature foaming process by adding aromatic thiols and epoxides.[71]

For optimal PCM performance within encapsulated PHU foams, it is essential to evaluate the thermophysical properties of PCMs, including melting/freezing temperatures, latent heat of fusion, specific heat capacity, thermal conductivity, thermal stability, and cyclic stability.[72] The PCM's phase transition temperature should align with the operating temperature range of the intended TES application.[72] A wide range of PCM types, such as organic, inorganic, and eutectic PCMs, can be considered for selecting the most suitable PCM.[73] The latent heat and heat capacity (related to energy density) quantify the amount of energy stored and released by the PCM, while thermal conductivity (related to power density) determines the rate of energy transfer within the PCM. Cyclic stability, assessed through multiple melt/freeze cycles, is crucial, especially for salt hydrate PCMs, which often require supercooling prevention for reversible phase transitions.[72,73] To enhance the thermophysical properties of PCMs, we integrated the PCMs into the PHU foam using a simple infiltration method. The inclusion of $BaCO_3$ has facilitated the cycling stability of $CaCl_2{\bullet}6H_2O$, a salt hydrate PCM. Additionally, graphite incorporation successfully improved the thermal conductivity of the PHU-encapsulated PCMs. When designing a TES system, a multi-layer approach incorporating graphite PHU foams (outer layers) and graphite-free PHU-encapsulated PCMs (inner layer) could be considered to leverage the high power density of graphite-infused foams and the high energy density of shape-stabilized PCMs.

Among various PCM applications,[8] the PHU-encapsulated PCMs described here hold promise for building materials and EV battery insulation. In building materials, PHU-encapsulated PCMs not only enable TES systems for space heating and cooling but also contribute to lightweight construction due to the inherent nature of polymeric foams.[8,9,16,20,53] For EV battery insulation, PCMs emerge as promising materials for maintaining battery efficiency across varying temperatures.[5,6] The lightweighting feature of PHU foams further complements battery insulation systems. Selecting the appropriate PCM phase transition temperature is critical. For instance, our $BaCO_3$-containing PHU-encapsulated $CaCl_2{\bullet}6H_2O$ system might be well-suited for lithium-ion battery insulation in EVs, considering the optimal operating temperature range of 15–35 °C.[74,75]

While this work serves as an initial proof-of-concept for the PHU-encapsulated PCMs in TES applications, technical challenges and limitations remain. The porous structure of PHU foams inherently allows for some PCM leakage upon melting. Additionally, the hygroscopic nature of PHUs leads to water absorption over time in atmospheric environments, potentially softening the foam and negatively impacting PCM thermal cycle behavior. These challenges presumably could be addressed by incorporating an outer barrier layer around the entire system to prevent leakage and water absorption – a crucial step for further prototype development. Furthermore, this work demonstrates the feasibility with only four PCM compounds (hexadecane, heptadecane, octadecane, and $CaCl_2{\bullet}6H_2O$). Future efforts should focus on optimizing the PHU formulation for various PCMs, including eutectic mixtures, to broaden the applicability of PCMs. Enhanced thermal conductivity through further investigation is also necessary to improve the efficiency of PCMs as TES materials. Finally, future work will involve demonstrating performance in targeted applications and developing an economical fabrication process at scale.

4. Conclusion

This study demonstrates the shape stabilization of PCMs through encapsulation within self-blowing and carbon-conscious PHU foams. To achieve successful foam formation, we optimized the formulation and curing conditions, investigating foam kinetics and morphology. This focus on formulation and processing resulted in PHU foams with mixed open and closed cells (diameter ≈300 µm), a glass transition temperature (T_g) of ≈ 15 °C, and a 5% weight loss decomposition temperature ($T_{d,\,5\%}$) of ≈ 220 °C. To evaluate the efficacy of PHU foams for PCM encapsulation, we infiltrated both paraffinic and salt hydrate PCMs into the foams and analyzed their thermal cycling behavior. While PHU-encapsulated paraffinic PCMs (hexadecane, heptadecane, octadecane) exhibited stable melting and freezing cycles, pure $CaCl_2{\bullet}6H_2O$ and its encapsulated form in PHU foam displayed no distinct melting or freezing transitions. However, we successfully achieved shape stabilization of $CaCl_2{\bullet}6H_2O$ by incorporating 5 wt.% $BaCO_3$ as a nucleating agent within the PHU foam. This approach yielded $BaCO_3$ PHU-encapsulated $CaCl_2{\bullet}6H_2O$ with stable melting and freezing behavior over 48 cycles.

We further investigated the effect of incorporating expanded graphite into the PHU foams to enhance the thermal conductivity of the encapsulated PCM system. The PHU foams with graphite resulted in an increased heating and cooling rate relative to the foam without graphite, indicating enhanced thermal conductivity. In conclusion, our work demonstrates the successful encapsulation of both organic and inorganic PCMs within PHU foams. These foams exhibit tunable thermal, chemical, and mechanical properties and maintain stable thermal cycles of PCMs for TES applications. This PHU-encapsulated PCM system provides a carbon-conscious material platform for designing future TES materials due to the greener synthetic path of PHUs (compared to traditional polyurethane synthesis) and tunability of PHU formulation and foaming process to accommodate various types of PCMs.

5. Experimental Section

Materials: Trimethylolpropane triglycidyl ether (TMPTGE) (Tech grade, CAS No. 3454-29-3) was sourced from BOC Sciences. Cabon dioxide (CO_2) gas (industrial grade) was sourced from Airgas. VORASURF^{TM} DC 5986 additive (surfactant) was sourced from Dow Chemical. Barium carbonate ($BaCO_3$) (99.78%, CAT No. 513-77-9) and calcium chloride hexahydrate ($CaCl_2{\bullet}6H_2O$) (99.2%, CAS No. 7774-34-7) were sourced from CHEM-IMPEX INT'L INC. Tetramethylene diamine (TMD) (>98.0%, CAS No. 110-60-1) and hexadecane (>98.0%, CAS No. 544-76-3) and octadecane (>98.0%, CAS No. 593-45-3) was purchased from TCI Chemicals. Other chemicals such as 2,2-(ethylenedioxy)diethanethiol (EDT) (95%, CAS No. 14970-87-7), 1,8-diazabicyclo[5.4.0]undec-7-ene (DBU) (≥ 99%, CAS No. 6674-22-2), tetrabutylammonium bromide (TBAB) (≥ 99%, CAS No. 1643-19-2), heptadecane (99%, CAS No. 629-78-7), and dichloromethane (≥ 99.5%, CAS No. 75-09-2) were purchased from Sigma–Aldrich. Graphite powder (synthetic, conducting grade, −200 mesh, 99.9995%, CAS No. 7782-42-5) was purchased from Alfa Aesar. Sodium sulfate (Na_2SO_4) (CAS No. 7757-82-6) was purchased from VWR chemicals.

Synthesis of Trimethylpropane Tricarbonate (TMPTC): To a 600 mL T316 stainless steel reaction cylinder, a 250 mL of TMPTGE (289.25 g, 0.9566 mol) was added first, and TBAB (28.9 g, 10 wt.%) was added. The loaded reaction vessel was properly fastened to the Parr reactor (equipped with a magnetically coupled stirring rod) according to the manufacturers protocol. While stirring, the reactor was pressurized with CO_2 and degassed 3 times to remove residual air. The vessel was pressurized to 500 psi with CO_2 and brought to 140 °C. The reactor was supplied with CO_2 throughout the course of the reaction as the gas was dissolved and consumed. The reaction was left to stir overnight. The cooled reaction mixture was transferred to a 1 L separatory funnel with ethyl acetate. The organic layer was extracted 3x with water, 1x with brine, and concentrated. To remove residual TBAB, the organic was redissolved in dichloromethane and extracted 3x with water, 1x with brine, and dried over Na_2SO_4 and concentrated and isolated as a pale-yellow viscous oil. The ^1H NMR spectrum was acquired using a Bruker 400 MHz spectrometer, as shown in Figure S1 (Supporting Information). The obtained data are consistent with literature reports.[42,76]

Preparation of PHU Foams: To the synthesized TMPTC (1 equiv) with the residual TBAB (0.005 equiv), EDT was added (0.45 equiv) and the viscous mixture was stirred. Next, DBU (0.1 equiv) and VORASURF^{TM} DC 5986 additive (Dow Chemical) (0.5 wt.% of the total mixture weight) were added. The mixture was stirred again until it became homogenous. Finally, TMD was added (1.025 equiv). The mixture was immediately stirred by hand for 10 min. Immediate aminolysis was observed as the mixture warmed and became more viscous. Next, the mixture was stirred by asymmetric centrifugal mixing (Flacktek Speedmixer) for 10 min at 3000 rpms. The reaction was left to sit in a closed container for 40 min ("precure" step), and then placed in an oven at 90 °C for 16 h. The final PHU foam was taken out and cooled down to room temperature for use. For the PHU foam with other additives, additives such as $BaCO_3$ (5 wt.% of the total mixture weight) and graphite (1.5 – 10 wt.% of the total mixture weight) were added before adding TMD and stirred until the mixture became homogenous.

Infiltration of PCMs into PHU Foams: PCMs including hexadecane, heptadecane, octadecane, and $CaCl_2{\bullet}6H_2O$ were melted above their melting point first. The PHU foam was immersed in the molten PCMs, taken out, and dried in the air until the PCMs were crystallized.

Rheology Measurement of PHU Foams: Rheological measurement was performed using stainless-steel parallel plates (D = 25 mm), with a 1 mm gap on the oscillatory rheometer (Discovery HR20 from TA instrument) for the sample mixtures, except the mixture of TMPTC and EDT. For the TMPTC and EDT mixture, the initial gap was set to 1.5 mm due to its low starting viscosity, which made it unsuitable for a 1 mm gap. The mixture was prepared following the section of preparation of PHU foams and loaded between two plates after the precure step for 40 min. Note that the final cure step for fabrication of PHU foam (i.e., curing at 90 °C) was performed using the rheometer instead of the oven. The measurement was performed in 2 steps including the temperature ramp from 25 °C to 90 °C with 20 °C min^{-1} of ramp rate at 2.5% of strain and 10 rad s^{-1} of angular frequency, and the curing at 90 °C for 120 min at 1.0% of strain and 10 rad s^{-1} of angular frequency. To simulate curing in the oven, the axial force was set to 0.0 N during the measurement. For samples cured at different temperatures (80 °C and 100 °C), the maximum test temperature was set to match the respective curing temperature (80 °C or 100 °C). The precure step was skipped for the sample shown in Figure 2A (TMPTC + TMD) due to its rapid increase in viscosity.

Characterization of PHU Foams—Scanning Electron Microscopy (SEM): The SEM samples were prepared following the section of the preparation of PHU foams. Both bare PHU foam and $BaCO_3$ PHU foam were sputtered with platinum (thickness = 5 nm) by Quorum Q150T S Plus, and then the SEM images were taken by Hitachi S-4800 under 3 kV.

Characterization of PHU Foams—Optical Microscopy (OM): The PHU foam samples were sectioned by hand to 1–3 mm using thin razor blades under magnification on a stereomicroscope. The bulk regions of the sectioned foam samples were imaged on a Nikon SMZ1500 stereomicroscope and captured with a Nikon DS-Fi1 CCD camera operated by a Nikon Digital Sight system (Nikon Instruments, Melville, NY). Helicon Focus (www.heliconsoft.com) was used to combine the in-focus regions of images captured at three different focal planes into a single, extended depth of focus image. With the sectioned foam samples, PCM was infiltrated as described above. The thermal cycle behavior of PHU-encapsulated octadecane, $BaCO_3$ PHU-encapsulated $CaCl_2{\bullet}6H_2O$, and graphite PHU-encapsulated octadecane were captured using a Linkham THMS600 (www.linkam.co.uk) in-situ microscopy heating stage. The temperature was controlled from 10 °C to 45 °C at a 2 °C min^{-1} ramp rate and then cooled back to 10 °C at a 1 °C min^{-1} ramp rate. Other experiments were performed with varying temperatures and ramps. Images were captured at a single focal plane every 0.5 °C and combined into a single movie file. For PHU-encapsulated octadecane and $BaCO_3$ PHU-encapsulated $CaCl_2{\cdot}6H_2O$ samples, a black background was used to maximize image contrast before and after PCM melting. For graphite PHU-encapsulated octadecane samples, a light-colored background (golden brass, corresponding to the color of the heating stage) was employed to enhance image contrast.

Characterization of PHU Foams—Digital Camera: The $BaCO_3$ PHU foam sample was manually sectioned into a circle shape with ≈3 mm thickness, 5 mm diameter using a razor blade. Following sectioning, $CaCl_2{\bullet}6H_2O$ was infiltrated into the foam as described above. The thermal cycle behavior of $BaCO_3$ PHU-encapsulated $CaCl_2{\bullet}6H_2O$ was captured using an iPhone 13 Pro running iOS 18 in High Efficiency Format (HEIF). The temperature was controlled between 10 °C and 65 °C at a 2 °C min^{-1} ramp rate and then cooled back to 10 °C with a varying ramp rate. Images were captured at intervals of 0.5–5 °C and compiled into a single video file.

Characterization of PHU Foams—Differential Scanning Calorimetry (DSC): For both bare PHU foam and $BaCO_3$-incorporated PHU foam ($BaCO_3$ PHU foam), the glass transition temperatures (T_g) were measured using DSC 25 (Discovery series) from the TA instrument. The measurement involved cooling the samples to −60 °C at a rate of 10 °C min^{-1}, followed by heating to 50 °C at the same rate (10 °C min^{-1}). An isothermal step of 5 min was held between the heating and cooling cycles.

The thermal cycling behavior of PCMs encapsulated within PHU foams was also measured using DSC 25 (Discovery series) from the TA instrument. The method involved establishing thermal equilibrium at 0 °C, followed by heating to 50 °C at a rate of 2 °C min^{-1}. The samples were then cooled back to 0 °C at a rate of 2 °C min^{-1} for paraffinic PCMs and $CaCl_2{\bullet}6H_2O$ in PHU foam, or 1 °C min^{-1} for $CaCl_2{\bullet}6H_2O$ in $BaCO_3$ PHU foam. As with the T_g measurements, an isothermal step of 5 min was included between each heating and cooling cycle.

Thermogravimetric Analysis (TGA): Thermal degradation of both bare PHU foam and $BaCO_3$ PHU foam was measured using TGA 5500 (Discovery series) from TA instrument by ramping temperature to 700 °C with the rate of 10 °C min^{-1} under nitrogen atmosphere.

Thermal Conductivity Meter: For the samples, 3 different types of PHU foams (bare PHU foam, the PHU foam with 5 wt.% of $BaCO_3$, and the PHU foam with 1.5 wt.% of graphite) were prepared. The foams were fabricated following the section of preparation of PHU Foams. To test the thermal conductivity of PHU foams with additives, a thermal conductivity meter, DTC-300 (model name) from TA instrument, equipped with Polyscience AD15R-40-A11B refrigerated circulator, and a liquid cell with a 2-inch diameter and 3.5 mm thickness, were used. Each sample was placed into a liquid cell with O-ring plate on the bottom, and the top plate was placed on top. A thin layer of thermal joint compound (TYPE 120 silicone, wakefield-vette) was applied to both the top and bottom plates of liquid cell before loading. The sample sandwiched between two plates was loaded on the lower surface plate of the test column and aligned. The top stack was then lowered, and the sample was checked to make sure it was in line with the top and bottom sample plates. Excess sink compound was wiped away from around the sample cell. Then the guard furnace was lowered and latched in place to begin testing. The thermal conductivity was measured in 6 different temperature points (0, 20, 40, 60, 80, and 100 °C). The chiller was turned on during the measurement.

Temperature Change Measurement of PHU Foams: For this measurement, 1–3 g of PHU foam was fabricated within 20 ml glass vials following the PHU foam preparation section. The asymmetric centrifugal mixing step was omitted due to the replacement of the speedmixer plastic cup with a glass vial for improved thermal conductance. PCMs were infused into the PHU foams by injecting the molten PCMs using a 6 ml syringe, followed by air drying until crystallization. To measure the temperature of both pure PCMs and PCM-infused PHU foams, a thermocouple connected to an EasyLog USB thermometer was inserted into the center of the foam. The PHU foam within the glass vial was subjected to 3 consecutive heating and cooling cycles. Each heating cycle was performed in a heating block on a hot plate at 60 °C for 20 min, followed by a cooling cycle in an ethylene glycol bath containing dry ice at ≈−10 °C for 20 min. The temperature of the cooling bath was maintained by adjusting the amount of dry ice. A total of 3 heating and cooling cycles were conducted. The temperature data for the samples was obtained from the EasyLog USB software.

Statistical Analysis: All data presented were processed without changes to create figures and tables. The data error bars and data presentation, such as mean ± SD, were obtained from duplicate or triplicate measurements of samples. Statistical tests were not used in this study.

Supporting Information

Supporting Information is available from the Wiley Online Library or from the author.

Acknowledgements

This work was authored by the National Renewable Energy Laboratory, operated by Alliance for Sustainable Energy, LLC, for the U.S. Department of Energy (DOE) under Contract No. DE-AC36-08GO28308. Funding was provided by NREL LDRD programs. The views expressed in the article do not necessarily represent the views of the DOE or the U.S. Government. The U.S. Government retains and the publisher, by accepting the article for publication, acknowledges that the U.S. Government retains a nonexclusive, paid-up, irrevocable, worldwide license to publish or reproduce the published form of this work or allow others to do so, for U.S. Government purposes.

Conflict of Interest

The authors declare no conflict of interest.

Author Contributions

M.L. and S.D.D. contributed equally to this work. S.D., N.A.R., and R.D.A. performed in conceptualization. S.D. and M.L. performed in formal analysis. N.A.R. and R.D.A. performed in funding acquisition. S.D., M.L., C.L., and B.S.D. performed in investigation and methodology. N.A.R. and R.D.A. performed in project administration and supervision. M.L. performed in visualization. S.D. and M.L. performed writing – original draft preparation. M.L., S.D., C.L., B.S.D., N.A.R., and R.D.A. performed in writing – review and editing. The manuscript was written through contributions of all authors and all authors have given approval to the final version of the manuscript.

Data Availability Statement

The data that support the findings of this study are available from the corresponding author upon reasonable request.

Keywords

non-isocyanate polyurethane, phase change materials, poly(hydroxy)urethane, reduced carbon materials, salt hydrate, thermal energy storage

Received: November 1, 2024
Revised: January 27, 2025
Published online: February 9, 2025

[1] *Global Status Report for Buildings and Construction*, The International Energy Agency (IEA), https://www.iea.org/reports/global-status-report-for-buildings-and-construction-2019 (accesses: December 2019).
[2] T. Kousksou, P. Bruel, A. Jamil, T. El Rhafiki, Y. Zeraouli, *Sol. Energy Mater. Sol. Cells* **2014**, *120*, 59.
[3] A. Sharma, V. V. Tyagi, C. R. Chen, D. Buddhi, *Renew. Sustain. Energy Rev.* **2009**, *13*, 318.
[4] J. Jaguemont, N. Omar, P. Van den Bossche, J. Mierlo, *Appl. Therm. Eng.* **2018**, *132*, 308.
[5] A. Wazeer, A. Das, C. Abeykoon, A. Sinha, A. Karmakar, *Energy Nexus* **2022**, *7*, 100131.
[6] A. H. Alami, H. M. Maghrabie, M. A. Abdelkareem, E. T. Sayed, Z. Yasser, T. Salameh, S. M. A. Rahman, H. Rezk, A. G. Olabi, *J. Energy Storage* **2022**, *54*, 105204.
[7] Y. Jing, Z. Zhao, X. Cao, Q. Sun, Y. Yuan, T. Li, *Nat. Commun.* **2023**, *14*, 8060.
[8] K. Pielichowska, K. Pielichowski, *Prog. Mater. Sci.* **2014**, *65*, 67.
[9] S. Ben Romdhane, A. Amamou, R. Ben Khalifa, N. M. Saïd, Z. Younsi, A. Jemni, *J. Build. Eng.* **2020**, *32*, 101563.
[10] R. K. Sharma, P. Ganesan, V. V. Tyagi, H. S. C. Metselaar, S. C. Sandaran, *Energy Convers. Manage.* **2015**, *95*, 193.
[11] D. C. Hyun, N. S. Levinson, U. Jeong, Y. Xia, *Angew. Chem. Int. Ed.* **2014**, *53*, 3780.
[12] N. Beaupere, U. Soupremanien, L. Zalewski, *Thermochim. Acta* **2018**, *670*, 184.
[13] X. Huang, X. Chen, A. Li, D. Atinafu, H. Gao, W. Dong, G. Wang, *Chem. Eng. J.* **2019**, *356*, 641.
[14] C. Cárdenas-Ramírez, F. Jaramillo, M. Gómez, *J. Energy Storage* **2020**, *30*, 101495.
[15] Y. Huang, A. Stonehouse, C. Abeykoon, *Int. J. Heat Mass Transfer* **2023**, *200*, 123458.
[16] A. Sivanathan, Q. Dou, Y. Wang, Y. Li, J. Corker, Y. Zhou, M. Fan, *Nanotechnol. Rev.* **2020**, *9*, 896.
[17] R. Jacob, F. Bruno, *Renew. Sustain. Energy Rev.* **2015**, *48*, 79.
[18] A. Jamekhorshid, S. M. Sadrameli, M. Farid, *Renew. Sustain. Energy Rev.* **2014**, *31*, 531.
[19] L. Liu, G. Alva, X. Huang, G. Fang, *Renew. Sustain. Energy Rev.* **2016**, *66*, 399.
[20] Z. Liu, Z. Yu, T. Yang, D. Qin, S. Li, G. Zhang, F. Haghighat, M. M. Joybari, *Build. Environ.* **2018**, *144*, 281.
[21] Y. Zhang, Z. Jia, A. Moqeet Hai, S. Zhang, B. Tang, *Composites, Part A* **2022**, *160*, 107047.
[22] G. A. Lane, *Sol. Energy Mater. Sol. Cells* **1992**, *27*, 135.
[23] R. Sharma, J. G. Jang, J. W. Hu, *Materials* **2022**, *15*, 335.
[24] P. Amoatey, K. Al-Jabri, S. Al-Saadi, *Int. J. Energy Res.* **2022**, *46*, 22386.
[25] K. Pielichowska, K. Nowicka-Dunal, K. Pielichowski, *Polymers* **2024**, *16*, 328.
[26] A. M. López-Sabirón, P. Royo, V. J. Ferreira, A. Aranda-Usón, G. Ferreira, *Appl. Energy* **2014**, *135*, 616.
[27] United Nations Environment Programme, Building Materials and the Climate: Constructing a New Future **2023**, ISBN: 978-92-807-4064-6.
[28] X. Huang, G. Alva, Y. Jia, G. Fang, *Renewable Sustainable Energy Rev.* **2017**, *72*, 128.
[29] F. Monie, B. Grignard, J.-M. Thomassin, R. Mereau, T. Tassaing, C. Jerome, C. Detrembleur, *Angew. Chem.* **2020**, *59*, 17033.
[30] F. Monie, B. Grignard, C. Detrembleur, *ACS Macro Lett.* **2022**, *11*, 236.
[31] M. S. Kathalewar, P. B. Joshi, A. S. Sabnis, V. C. Malshe, *RSC Adv.* **2013**, *3*, 4110.
[32] A. Gomez-Lopez, F. Elizalde, I. Calvo, H. Sardon, *Chem. Commun.* **2021**, *57*, 12254.
[33] H. Khatoon, S. Iqbal, M. Irfan, A. Darda, N. K. Rawat, *Prog. Org. Coat.* **2021**, *154*, 106124.
[34] M. Mangal, H. Supriya, S. Bose, T. Banerjee, *Biopolymers* **2023**, *114*, e23568.
[35] T. Dong, E. Dheressa, M. Wiatrowski, A. P. Pereira, A. Zeller, L. M. L. Laurens, P. T. Pienkos, *ACS Sustainable Chem. Eng.* **2021**, *9*, 12858.
[36] M. Desroches, M. Escouvois, R. Auvergne, S. Caillol, B. Boutevin, *Polym. Rev.* **2012**, *52*, 38.
[37] Mhd. M. A. C. Haniffa, K. Munawar, Y. C. Ching, H. A. Illias, C. H. Chuah, *Chem. - Asian J.* **2021**, *16*, 1281.
[38] L. Maisonneuve, O. Lamarzelle, E. Rix, E. Grau, H. Cramail, *Chem. Rev.* **2015**, *115*, 12407.
[39] T. Hassan, A. Salam, A. Khan, S. U. Khan, H. Khanzada, M. Wasim, M. Q. Khan, I. S. Kim, *J. Polym. Res.* **2021**, *28*, 36.
[40] S. Hu, X. Chen, J. M. Torkelson, *ACS Sustainable Chem. Eng.* **2019**, *7*, 10025.
[41] D. J. Fortman, J. P. Brutman, C. J. Cramer, M. A. Hillmyer, W. R. Dichtel, *J. Am. Chem. Soc.* **2015**, *137*, 14019.
[42] N. S. Purwanto, Y. Chen, T. Wang, J. M. Torkelson, *Polymer* **2023**, *272*, 125858.

[43] V. Froidevaux, C. Negrell, S. Caillol, J. P. Pascault, B. Boutevin, *Chem. Rev.* **2016**, *116*, 14181.
[44] S. R. Nicholson, N. A. Rorrer, T. Uekert, G. Avery, A. C. Carpenter, G. T. Beckham, *ACS Sustainable Chem. Eng.* **2023**, *11*, 2198.
[45] Z.-G. Qian, X.-X. Xia, S. Y. Lee, *Biotechnol. Bioeng.* **2009**, *104*, 651.
[46] M. North, R. Pasquale, *Angew. Chem. Int. Ed.* **2009**, *48*, 2946.
[47] P. S. Choong, N. X. Chong, E. K. Wai Tam, A. M. Seayad, J. Seayad, S. Jana, *ACS Macro Lett.* **2021**, *10*, 635.
[48] K. Błażek, H. Beneš, Z. Walterová, S. Abbrent, A. Eceiza, T. Calvo-Correas, J. Datta, *Polym. Chem.* **2021**, *12*, 1643.
[49] P. Parcheta-Szwindowska, K. Rohde, J. Datta, *J. Therm. Anal. Calorim.* **2022**, *147*, 13329.
[50] Y. Xia, W. Cui, H. Zhang, F. Xu, L. Sun, Y. Zou, H. Chu, E. Yan, *J. Mater. Chem. A* **2017**, *5*, 15191.
[51] J. Yang, X. Li, S. Han, Y. Zhang, P. Min, N. Koratkar, Z.-Z. Yu, *J. Mater. Chem. A* **2016**, *4*, 18067.
[52] P. Dixit, V. J. Reddy, S. Parvate, A. Balwani, J. Singh, T. K. Maiti, A. Dasari, S. Chattopadhyay, *J. Energy Storage* **2022**, *51*, 104360.
[53] R.-J. Clark, A. Mehrabadi, M. Farid, *J. Energy Storage* **2020**, *27*, 101145.
[54] D. Ibbotson, S. Ahmed, P. J. Shamberger, *J. Phys. Chem. C* **2024**, *128*, 17282.
[55] B. Tang, L. Wang, Y. Xu, J. Xiu, S. Zhang, *Sol. Energy Mater. Sol. Cells* **2016**, *144*, 1.
[56] D. V. Voronin, E. Sitmukhanova, R. I. Mendgaziev, M. I. Rubtsova, D. Kopitsyn, K. A. Cherednichenko, A. P. Semenov, R. Fakhrullin, D. G. Shchukin, V. Vinokurov, *Materials* **2023**, *16*, 6460.
[57] H. Hu, *Composites, Part B* **2020**, *195*, 108094.
[58] K. Yu, Y. Liu, Y. Yang, *Appl. Energy* **2021**, *292*, 116845.
[59] P. Karimineghlani, E. Emmons, M. J. Green, P. Shamberger, S. A. Sukhishvili, *J. Mater. Chem. A* **2017**, *5*, 12474.
[60] L. UT-Battelle, (US Patent Application Publication), US2021/0340423 A1, **2021**.
[61] S. Zhang, D. Feng, L. Shi, L. Wang, Y. Jin, L. Tian, Z. Li, G. Wang, L. Zhao, Y. Yan, *Renewable Sustainable Energy Rev.* **2021**, *135*, 110127.
[62] B. K. Purohit, V. S. Sistla, *J. Energy Storage* **2017**, *12*, 196.
[63] B. K. Purohit, V. S. Sistla, *Thermochim. Acta* **2018**, *668*, 9.
[64] F. Meng, M. Brandao, J. M. Cullen, *Environ. Sci. Technol.* **2024**, *58*, 2716.
[65] X. Zhang, Y. Kim, D. Kim, M. Liu, I. B. V. Erramuspe, G. B. Kaya, X. Wang, T. Kim, B. K. Via, H. Cho, *ACS Appl. Energy Mater.* **2020**, *4*, 416.
[66] W. Aftab, A. Mahmood, W. Guo, M. Yousaf, H. Tabassum, X. Huang, Z. Liang, A. Cao, R. Zou, *Energy Storage Mater.* **2019**, *20*, 401.
[67] T. Wang, H. Deng, H. Zeng, J. Shen, F. Xie, C. Zhang, *ACS Sustainable Resour. Manage.* **2024**, *1*, 462.
[68] J. Sternberg, S. Pilla, *Green Chem.* **2020**, *22*, 6922.
[69] M. Bourguignon, B. Grignard, C. Detrembleur, *Angew. Chem. Int. Ed.* **2022**, *61*, 202213422.
[70] D. Trojanowska, F. Monie, G. Perotto, A. Athanassiou, B. Grignard, E. Grau, T. Vidil, H. Cramail, C. Detrembleur, *Green Chem.* **2024**, *26*, 8383.
[71] M. Bourguignon, B. Grignard, C. Detrembleur, *Polym. Chem.* **2024**, *16*, 192.
[72] H. Nazir, M. Batool, F. J. Bolivar Osorio, M. Isaza-Ruiz, X. Xu, K. Vignarooban, P. Phelan, Inamuddin, A. M. Kannan, *Int. J. Heat Mass Transfer* **2019**, *129*, 491.
[73] X. Wang, W. Li, Z. Luo, K. Wang, S. P. Shah, *Energy Build.* **2022**, *260*, 111923.
[74] F. S. Hwang, T. Confrey, C. Reidy, D. Picovici, D. Callaghan, D. Culliton, C. Nolan, *Renewable Sustainable Energy Rev.* **2024**, *192*, 114171.
[75] S. Kharabati, S. Saedodin, *J. Energy Storage* **2024**, *75*, 109586.
[76] S. Panchireddy, J. M. Thomassin, B. Grignard, C. Damblon, A. Tatton, C. Jerome, C. Detrembleur, *Polym. Chem.* **2017**, *8*, 5897.

